Ultrafast Energy Relaxation Dynamics of Directly Linked Porphyrin Arrays

Hyun Sun Cho,† Nam Woong Song, Yong Hee Kim, Sae Chae Jeoung, Sangjoon Hahn, and Dongho Kim*

National Creative Research Initiatives Center for Ultrafast Optical Characteristics Control and Spectroscopy Laboratory, Korea Research Institute of Standards and Science, Taejon 305-600, Korea

Seong Keun Kim

Department of Chemistry, Seoul National University, Seoul 151-742, Korea

Naoya Yoshida and Atsuhiro Osuka*

Department of Chemistry, Graduate School of Science, Kyoto University, Kyoto 606-8502, Japan

Received: December 6, 1999

A variety of porphyrin arrays connected together with different linkage were devised for possible applications to molecular optoelectronic devices such as wires, logic gates, and artificial light-harvesting arrays, etc. It has been relatively well established that the light signal transmission in these molecular assemblies is based on exciton migration process, which possibly gives rise to the structural changes during the exciton delocalization process. Zinc(II) 5,15-di(3,5-di-*tert*-butylphenyl)porphyrin (Z1), its directly meso,meso-linked porphyrin dimer (Z2), trimer (Z3), and tetramer (Z4) were synthesized with the goal to elucidate the relationship between exciton migration and structural change upon photoexcitation. One of the most important factors in structural changes for these porphyrin arrays is mainly determined by the dihedral angle between adjacent porphyrin moieties. For a systematic approach toward the investigation of the exciton coupling dynamics influenced by the relative orientation between neighboring porphyrin molecules, various time-resolved spectroscopic techniques such as fluorescence decay and transient absorption measurements with different polarization in pump/probe beams have been utilized. The steady-state excitation anisotropy spectra of Z2, Z3, and Z4 porphyrin arrays show that the photoexcitation of the high-energy exciton Soret band induces a large angle change between absorption and emission dipoles in contrast with the photoexcitation of the low-energy exciton split Soret and Q-bands. In the order of Z1, Z2, Z3, and Z4, their S_1 states decay faster because of the increasing energy dissipation processes into a larger number of accessible states. In contrast, the rotational diffusion rates become slower in the same order because the overall molecular shape is elongated along the long axis of the molecular arrays, which experiences a large displacement of solvent molecules in rotational diffusion motion. Ultrafast fluorescence decay measurements show that the $S_2 \rightarrow S_1$ internal conversion process occurs in less than 1 ps in Z2, Z3, and Z4 due to the existence of exciton split band as a ladder-type deactivation channel, while this process is relatively slow in Z1 ($\sim$1.6 ps). Femtosecond transient absorption experiments with magic angle and different polarization in probe beam were performed to find the relationship between energy relaxation and anisotropy dynamics upon photoexcitation. The internal conversion in Z2, Z3, and Z4 is likely to be accompanied by the incoherent energy hopping processes occurring in less than $\sim$200 fs judging from a large change in the anisotropy value in the transient absorption decay. In addition, the decay components with approximately 8 ps time constant were observed in both fluorescence up-conversion and femtosecond transient absorption decays. These components are believed to arise from the conformational change in the excited states, because the dihedral angle distribution in these arrays was estimated to be $90° \pm 20°$ at ambient temperature from the AM1 calculation.

I. Introduction

The light-harvesting array complexes[1] constituting the photosynthetic organisms transfer solar energy to the reaction center.[2] It is well established that light-harvesting complexes are very efficient in the energy transfer process, although it occurs over long distances. The elucidation of the factors determining the efficiency of naturally occurring light-harvesting array systems is a longstanding objective of photosynthesis research although it often meets lots of difficulties due to the size and complexity of the assemblies. Understanding the structural and electronic properties of natural light-gathering arrays that give rise to efficient energy transfer is prerequisite for elicit molecular design for the realization of molecular devices in molecular semiconductors[3] and conductors,[4] catalytic reduction of dioxygen to water,[5] photovoltaic energy conversion/charge storage,[6] and optical sensing.[7] For this purpose, synthetic tetrapyrrole-based molecular model systems such as chloro-

* To whom correspondence should be addressed.
† Also with Department of Chemistry, Seoul National University, Seoul 151-742.

10.1021/jp9942623 CCC: $19.00
Published on Web 03/29/2000

phylls,[8] porphyrins,[9] phthalocyanines,[10] and their metallo derivatives are suitable for probing the effects of molecular organization on electronic interaction.

Various types of covalently linked arrays of metalloporphyrins have been designed and synthesized with the goal of applying these molecular oligomers to molecular photonic devices and artificial biomimetic light-harvesting array systems. In addition to achieving highly efficient energy transfer, for systematic study, such systems must possess organic solubility and architectural rigidity and allow the incorporation of many porphyrinic pigments in precise states of metalation and geometrical arrangement. Since the preparation and purification of molecular assembly is indeed an intensive labor-consuming work, the ability to predict reliably the performance characteristics of aimed molecular photonic devices is very highly desirable. There has been a great advance in synthesizing numerous multiporphyrin light-harvesting array architectures especially with distinct linkage interconnecting porphyrin molecular species. Multiporphyrin arrays have been constructed using several types of shorter linkers that are suitable for preparing linear or extended architectures via meso position attachment. Various synthetic strategies have been developed in order to make multiporphyrin oligomers with linear, cyclic, and cross-linked geometries. These include porphyrins joined by ethene,[11] ethyne,[12] butadiyne,[12−15] furan,[13] enyne,[15] hexatriene,[16] *p*-phenylene,[17] phenylethene,[18] naphthalene,[19] biphenyl,[19,20] phenanthrene,[19] and ethynylphenylethyne[15] groups. The recent progress in synthesizing capabilities of various porphyrin arrays raises a fundamental question regarding the photophysical properties and molecular architecture relationship such as energy migration/gradient. The number of pigments, spectral and electronic properties of pigments, and linkage structure have a strong influence on the overall photophysical properties of porphyrin oligomers.

The exciton coupling strength mainly governed by the interconnection length between porphyrin molecules is one of the most distinct phenomena occurring in molecular assembly. For instance, multiporphyrin arrays incorporating a diarylethyne linkage exhibit a relatively rigid structure with ∼20 Å center-to-center distance.[21] These types of porphyrin arrays are believed to be weakly coupled to each other because the absorption spectra are essentially composed of individual pigment, indicating a weak electronic communication among constituent pigments. In contrast, the attachment of porphyrins via ethyne[12] or butadiyne[12−15] units results in a strong electronic coupling as evidenced by a split in the Soret (B) band and an effective π-conjugation as seen in the dramatic red-shift of the Q-bands. These interactions are more significant in the Soret region due to the large transition dipole moment associated with these transitions and are manifest in the pronounced spectral splitting over 400−500 nm energy domain. This indicates that as semirigid ethyne or butadiyne linkers are employed, the in-plane structure of the porphyrin arrays becomes favorable in the ground state.

Furthermore, the direct meso−meso connection results in a stronger electronic coupling causing a further split in the Soret band.[22] However, the Q-bands of these porphyrin arrays are much less perturbed due to poor electronic communication imposed by the orthogonality of the adjacent porphyrins. A directly linked bridge enforces a large dihedral angle between each constituent; the calculated minimum energy torsional angle for this species resides around at 90°. While this near-orthogonal orientation of the (porphinato)zinc(II) units of the dimer, trimer, and tetramer restricts *inter*-ring π-conjugation, it allows for

SCHEME 1

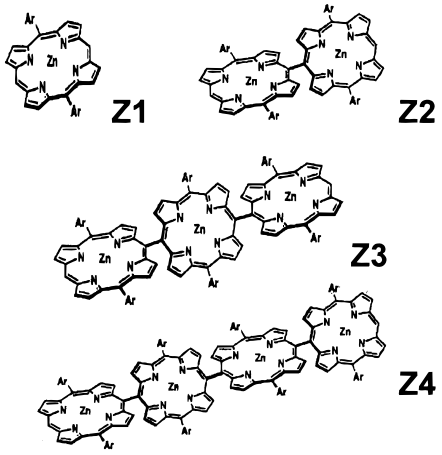

Ar = 3,5-di-*tert*-butylphenyl

mixing of the electronic states of each monomer by excitonic interactions. This observation also indicates that the dominant low-energy component in the solution spectrum arises from an orthogonal structure in addition to the existence of vibronic states. This unique property in these types of porphyrin arrays attracts much attention, especially the energy flow mechanism upon photoexcitation accompanied by the relative orientational motion related to the dihedral angle between the adjacent porphyrin moieties. Up to now, the construction of this connection is known to lack synthetic control. But it became possible to connect the porphyrin molecules directly up to four porphyrin units (Scheme 1).[22]

In order to investigate the photophysical properties of directly linked (porphinato)zinc(II) systems, it is important to consider the range of sterically accessible chromophore−chromophore dihedral angles at ambient temperature and the porphyrin-to-porphyrin linkage topology in the ground and excited states.[23] The possibility for the presence of additional, presumably nonorthogonal, conformers in solution which absorb at slightly different energies is expected to be minimal. In other words, the distribution for the different conformers in terms of the dihedral angle should be narrow. On the contrary, the pronounced intensification and the red shift of the lowest energy absorption bands observed for the meso-to-meso ethyne-bridged dimer and trimer are indicative of increased conjugation, stabilizing transitions which are polarized along the long axis of these molecules.[12]

With these objectives in this investigation, the directly linked zinc(II) porphyrin dimer, trimer, and tetramer along with their corresponding monomer are employed to investigate the difference in the exciton coupling dynamics accompanied by the relative orientational motion between the two porphyrin rings. For a systematic approach, we have performed steady-state anisotropy measurements to have structural information on these porphyrin oligomers. The fluorescence anisotropy decay was conducted to explore the rotational diffusion related to molecular structures along with the decay of the lowest excited emitting state. The femtosecond fluorescence up-conversion measurement was done to investigate the formation dynamics of the lowest excited emitting state and the contribution of the heterogeneity in the conformational distribution of these porphyrin arrays. Finally, femtosecond transient absorption experiments with different polarizations in the probe beam were carried out in

order to observe the anisotropy decay at the initial stage of exciton migration process upon photoexcitation.

II. Experimental Methods

The zinc(II) 5,15-di(3,5-di-*tert*-butylphenyl)porphyrin (Z1), its meso,meso-linked porphyrin dimer (Z2), trimer (Z3), and tetramer (Z4) were synthesized.[22] Spectroscopic grade tetrahydrofuran and toluene were used as solvent for all experiments. The absorption spectra were recorded by using a Varian Cary 3 spectrophotometer, and fluorescence measurements were made on a scanning SLM-AMINCO 4800 spectrofluorometer, which makes possible to obtain the corrected spectra using rhodamine B as a quantum counter. Steady-state fluorescence anisotropy spectra were obtained by changing the detection polarization on fluorescence path parallel or perpendicular to the polarization of the exciting light. Then anisotropy values were calculated as follows:

$$r = \frac{I_{VV} - GI_{VH}}{I_{VV} + 2GI_{VH}}$$

where I_{VV} (or I_{VH}) is the signal intensity when the excitation light is vertically polarized and only vertically (or horizontally) polarized portion of fluorescence is detected, denoting that the subscripts stand for excitation and detection polarization, respectively. The factor G is defined by I_{HV}/I_{HH} which is equal to the ratio of the sensitivities of the detection system for vertically and horizontally polarized light.

The picosecond time-resolved fluorescence experiments were carried out by using time correlated single photon counting (TCSPC) method.[24] The picosecond excitation pulses at 563 nm were obtained from a cavity-dumped picosecond dye laser (Coherent 702) synchronously pumped by a mode-locked Ar ion laser (Coherent Innova 200). The cavity dumped beam from the dye laser has 2 ps pulse width and an average power of ca. 40 mW at 3.8 MHz dumping rate when rhodamine 6G for gain dye was used. The excitation pulses at 410 nm were obtained from a femtosecond Ti:sapphire laser (Coherent, MIRA) with an average power of 600 mW at 820 nm. The pump pulses at desired wavelength were generated by frequency doubling with a β-BBO crystal. The emission was collected at a 45° angle with respect to the excitation laser beam by 5 and 25 cm focal length lenses, focused onto a monochromator (Jovin-Yvon HR320), and detected with a microchannel plate photomultiplier tube (Hamamatsu R2809U). The signal was amplified by a wideband amplifier (Philip Scientific), sent to a Quad constant fraction discriminator (Tennelec), a time-to-amplitude converter (Tennelec), a counter (Ortec), and a multichannel analyzer (Tennelec/Nucleus), and stored in a computer. The time-dependent anisotropy decay was obtained by using the polarizer and depolarizer before the detection system.

The light source for fluorescence up-conversion measurement[25] was a mode-locked Ti:sapphire laser (Coherent, MIRA-900F) pumped by a intracavity frequency-doubled cw Nd:YVO_4 laser (Coherent, Verdi) with an average power of 550 mW and ~120 fs pulse width at 800 nm. The second harmonic pulses (λ = 400 nm, 140 mW) were generated by using a β-BBO (1 mm thick) crystal. The residual fundamental pulses after the dichroic mirror were used as the gate pulses for the up-conversion of fluorescence. The time interval between the fluorescence and gate pulses was controlled by a delay stage equipped with a corner cube gold retroreflector (Coherent, 2 in. diameter) for travelling the gated pulse. The excitation laser beam was focused onto the sample by using a 10 cm focal length quartz lens, and its power was controlled by using a variable neutral-density filter. The fluorescence is collected and focused onto a β-BBO (1 mm thick, type-I) crystal for the up-conversion by using an aluminum coated parabolic mirror (Coherent, 5 and 20 cm in focal lengths). A cutoff filter (Schott Glass Filter Co., GG455, 1 mm thick) was placed between collimating and focusing mirrors to remove the transmitted pump pulse. Up-converted signals were focused onto the entrance slit of a 32 cm focal length monochromator (Jovin Yvon, HR320) after passing through a UV band-pass filter (Schott Glass Filter Co., UG11). The signal was detected by a head-on type photomultiplier tube (Hamamatsu, model 3235) with a gated photon counter (Stanford Research Systems, SR400). The gated photon counter was interfaced with a personal computer which controls the delay stage. The full width at half-maximum value of the cross-correlation trace between the excitation and gate pulses was estimated to be ~280 fs, which determines the time resolution of the fluorescence up-conversion measurements.

The dual beam femtosecond time-resolved transient absorption spectrometer[26] consisted of a self-mode-locked femtosecond Ti:sapphire laser (Coherent, MIRA), a Ti:sapphire regenerative amplifier (Quantronix) pumped by a Q-switched Nd:YLF laser, a pulse stretcher/compressor, and an optical detection system. A femtosecond Ti:sapphire oscillator pumped by a cw Nd:YVO_4 laser (Coherent, Verdi) produces a train of 60 fs mode-locked pulses with an average power of 600 mW at 800 nm. The seed pulses from the oscillator were stretched (~250 ps) and sent to a Ti:sapphire regenerative amplifier pumped by a Q-switched Nd:YLF laser operating at 1 kHz. The femtosecond seed pulses and Nd:YLF laser pulses were synchronized by adjusting an electronic delay between Ti:sapphire oscillator and Nd:YLF laser. Then the amplified pulse train inside the Ti:sapphire regenerative amplifier was cavity-dumped by using the Q-switching technique, and about 30 000-fold amplification at 1 kHz was obtained. After compression, the resulting laser pulses had a pulse width of ~100 fs and an average power of 1 W at 1 kHz repetition rate in the range of 790−840 nm. These pulses were split into two beams by using the beam splitter. One was used as the pump beam by frequency doubling in a β-BBO crystal. The other was focused onto a flowing water cell to generate a white light continuum, which was again split into two parts. One part of the white light continuum was overlapped with the pump beam at the sample to probe the transient, while the other part of the beam was passed through the sample without overlapping the pump beam. The monitoring wavelength was selected by putting an appropriate interference filter (fwhm = 10 nm). By chopping the pump pulses at 43 Hz, the modulated probe pulse as well as the reference pulse was detected by photodiodes. The output current was amplified with a homemade fast preamplifier, and then the resultant voltage of the probe pulses was normalized by a boxcar averager with pulse-to-pulse configuration. The resultant signal modulated by a chopper was measured by a lock-in amplifier and then fed into a personal computer for further signal processing.

The sample was circulated by using the flow cell (1 mm path length) to minimize the signal change by sample degradation and thermal lens effect in both fluorescence up-conversion and transient absorption experiments.

III. Results

Steady-State Fluorescence Anisotropy. Figure 1 shows the absorption spectra of monomeric, dimeric, trimeric and tetrameric zinc(II) porphyrins (Z1, Z2, Z3, Z4) in THF, which denotes the interesting systematic changes in the Soret bands

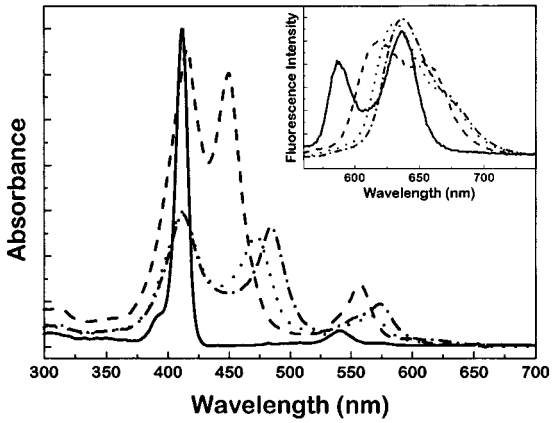

Figure 1. Absorption and fluorescence (inset) spectra of Z1 (—), Z2 (– – –), Z3 (•••) and Z4 (•-•-•) in THF.

TABLE 1: Emission Anisotropy Decay Parameters for Z1, Z2, Z3, and Z4

compound	λ_{ex}	λ_{em}	τ(ns)	r_0	Φ (ns)	δ	r
Z1	560	586	2.57	0.23	0.3	32	0.025 (0.023)[a]
	410			0.13	0.2	42	0.01 (0.018)
Z2	563	618	1.93	0.19	0.5	36.4	0.03 (0.028)
	410			−0.05	0.43	60	−0.01 (−0.015)
Z3	568	632	1.58	0.19	0.7	36	0.06 (0.064)
	410			−0.08	0.64	63	−0.03 (−0.03)
Z4	575	634	0.92	0.28	1.1	26	0.15 (0.13)
	410			−0.03	1.0	58	−0.01 (−0.03)

[a] Estimated from steady-state polarized excitation spectra.

with an increase in the number of porphyrin moieties. While the Soret band of Z1 exhibits a single absorption maximum at 415 nm, that of Z2 is split into two bands with absorption peaks at 421 and 457 nm. In the cases of Z3 and Z4, the splitting of the Soret band becomes more significant, exhibiting two Soret bands at 413 and 472 nm in Z3 and at 413 and 485 nm in Z4, respectively. These systematic changes can be explained in terms of exciton coupling theory. The fluorescence spectra of Z1 exhibit vibronic emission bands at 587 and 637 nm (inset of Figure 1). As the number of porphyrin ring units increases, the dual emission bands of Z1 are red-shifted with a decrease in the relative intensity of the low-energy vibronic emission band. In parallel with these changes, the fluorescence lifetimes decrease without any changes in the lifetimes depending on excitation and monitoring wavelengths (Table 1).

The anisotropy of an optical experiment is widely used to provide information about the alignment dynamics occurring after excitation of a system. The anisotropy is often defined as the difference between the detector response when the pump and signal fields are polarized parallel and orthogonal ($I_{||} - I_{\perp}$) divided by the omnidirectional signal ($I_{||} + 2I_{\perp}$). Such measuremnts have proven to be valuable adjuncts to ultrafast kinetic measurements in studies of rotational diffusion,[27] energy transfer,[28] analysis of kinetic schemes,[29] reactant−product alignment in solution phase reactions,[30] and vibrational excitation experiments,[31] and in numerous other applications.[32]

In order to obtain information on the orientation of transition dipoles of Z1, Z2, Z3, and Z4, we have measured the fluorescence excitation anisotropy spectra (Figure 2a). The fluorescence excitation anisotropy of the monomeric porphyrin Z1 turns out to be positive regardless of the excitation wavelength, because both absorption and emission oscillators are polarized in the same plane. In the cases of Z2, Z3, and Z4 porphyrin arrays, however, we obtained negative anisotropy values in the fluorescence excitation anisotropy spectra around

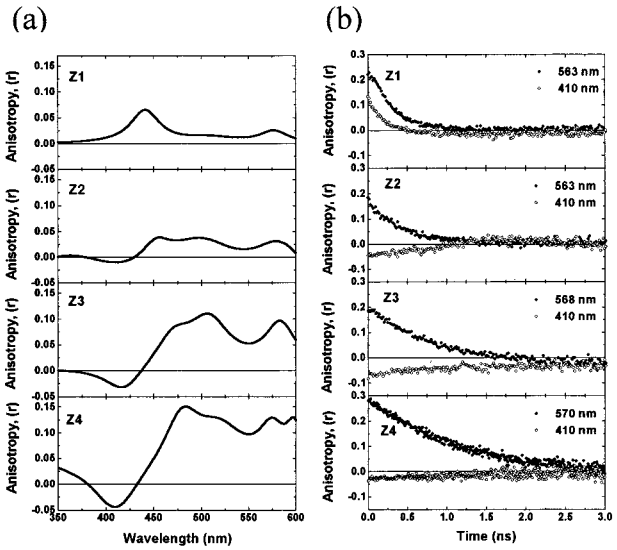

Figure 2. (a) Steady-state excitation anisotropy spectra and (b) the fluorescence anisotropy decay profiles of Z1, Z2, Z3, and Z4.

at 415 nm which corresponds to one of the split Soret bands. The anisotropy values above 450 nm for this series of porphyrin arrays are positive and the difference between the anisotropy values of around 415 nm and the entire visible region becomes larger as the number of porphyrin rings increases. We have also carried out the time-resolved fluorescence anisotropy measurements to have information on molecular reorientational motion and excitation energy transfer of Z1, Z2, Z3, and Z4 (Figure 2b). Excitation wavelengths were selected in resonance with B (410 nm) and Q-bands (563 nm), and the emission detection wavelengths were 586, 618, 632, and 634 nm for Z1, Z2, Z3, and Z4, respectively. The emission anisotropy decay appeared to be single exponential at all excitation wavelengths with a significant decrease in relaxation rates with an increase in the number of porphyrin moieties (Table 1). The initial anisotropy (r_0) values of these porphyrin arrays are observed to be dependent on the excitation wavelength. The r_0 values in Z2, Z3, and Z4 exhibit the negative sign with an excitation at 410 nm whereas the positive values are obtained with an excitation at Q-band. However, the r_0 values in Z1 are all positive regardless of excitation wavelength. Therefore, in the cases of Z2, Z3, and Z4 at $\lambda_{ex} = 410$ nm, there exists a large difference in orientation angle between absorption and emission dipoles due, in large part, to incoherent energy hopping processes from one porphyrin moiety to another, which are aligned orthogonal to each other in these molecular arrays. On the basis of the initial anisotropy values (r_0) of the time-resolved anisotropy data, the average angle δ between absorption and emission dipoles can be estimated according to the equation $r_0 = 0.2(3\cos^2\delta - 1)$ (Table 1). In addition, we have calculated the anisotropy value, r, using the Perrin equation.[33]

$$r = \frac{r_0}{1 + (\tau/\Phi)}$$

where r_0 is the initial anisotropy value, Φ is the anisotropy decay time, and τ is the fluorescence lifetime. The anisotropy values calculated from the time-resolved anisotropy decay are in a good agreement with those obtained from the steady-state excitation anisotropy spectra (Figure 2 and Table 1).

Ultrafast Fluorescence Decay of Z1, Z2, Z3, and Z4. The fluorescence decay profile of Z1 probed at 640 nm after photoexcitation at 400 nm exhibits the rise component with 1.6

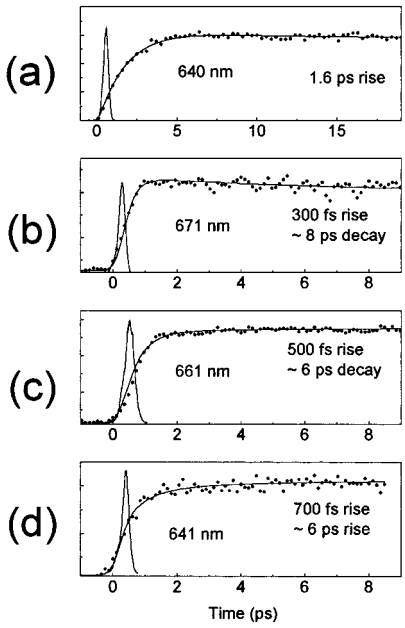

Figure 3. Fluorescence up-conversion decay profiles of (a) Z1 at 640 nm, (b) Z2 at 671 nm, (c) Z3 at 661 nm, and (d) Z4 at 641 nm after the photoexcitation at 400 nm. The delta-function-like solid lines represent the IRF (instrumental response function) based on the cross-correlation function.

ps time constant corresponding to a relatively slow $S_2 \rightarrow S_1$ internal conversion process (Figure 3a). It is already established that the S_2 states of 5,10,15,20-tetraphenyl and 5,15-diphenyl zinc porphyrin analogues are relatively long-lived with lifetimes of 1−2 ps.[34,35] Since Z1 compound is zinc(II) 5,15-di(3,5-di-*tert*-butylphenyl)porphyrin, the 1.6 ps lifetime of the S_2 state seems to be quite reasonable. Furthermore, the fluorescence decay profile observed at 460 nm, which is believed to be $S_2 \rightarrow S_0$ fluorescence, exhibits a single-exponential decay with 1.2 ps time constant. The probe wavelength dependence of fluorescence decay of Z1 between 530 and 600 nm shows both rise and decay profile with the increase of both time constants as the probe wavelength increases. This result indicates the existence of the vibrational energy redistribution process in the S_1 state manifolds. A little difference in $S_2 \rightarrow S_0$ decay time (1.2 ps, 460 nm probe) and $S_1 \rightarrow S_0$ rise time (1.6 ps, 640 nm probe) can be understood as due to the retardation of the vibrational energy redistribution rate in the low-lying vibrational states in S_1 manifolds. This 1.6 ps rise time does not seem to be due to the result of vibrational cooling which occurs via solvent−solute interaction since this process in the S_1 states of porphyrin monomers occurs on the time scale of 10−20 ps.[36,37] Thus, our observation implies that the 1.6 ps time constant is mainly attributable to both the internal conversion process of the S_2 state decaying to the S_1 state and the vibrational energy redistribution in S_1 manifolds.

Figure 3b also shows the temporal profile of fluorescence signal in Z2 observed at 671 nm, illustrating about 300 fs initial and a subsequent fast decay with approximately 8 ps time constant. Under this fast decay process, a plateau arising from the long-lived S_1 state having 1.93 ns lifetime, as revealed by the TCSPC method, contributes to the overall decay signal in this short time window. The temporal profile of Z3 fluorescence at 661 nm also exhibits an initial rise component of about 500 fs, followed by a fast decay component with about 6 ps time constant as observed in Z2 (Figure 3c). The decay process representing the S_1 state decay with a lifetime of 1.58 ns should also contribute to the overall decay profile as a plateau in this short time window. The fluorescence decay profile in Z4 at 641 nm exhibits about 700 fs and ~6 ps rise components. The overall temporal decay profile is believed to be contributed by a long-lived S_1 state of Z4 with about 0.92 ns lifetime (Figure 3d).

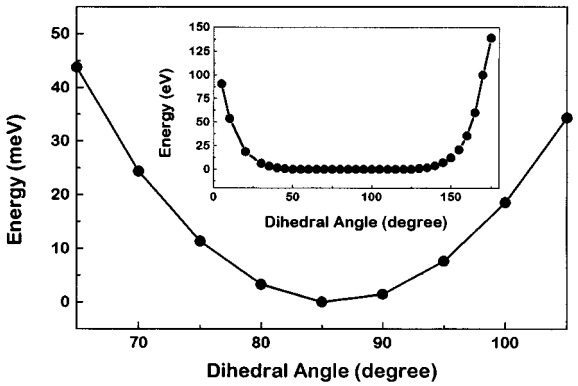

Figure 4. Ground-state energy change of Z2 depending on the dihedral angle calculated by AM1 method.

The $S_2 \rightarrow S_1$ internal conversion rate increased from Z1 (~1.6 ps) to Z2 (~300 fs), Z3 (~500 fs), and Z4 (~700 fs) in porphyrin moieties. This result suggests that the existence of the exciton split band (S_2') between monomeric Soret band around at 415 nm and Q-bands in visible region provides ladder-type deactivation channels after photoexcitation at 400 nm which increases the overlap integral between the upper electronic S_2 states and the lowest excited S_1 state.

The ~8 ps decay component of Z2 and the ~6 ps rise components of Z3 and Z4 in the fluorescence temporal profiles probably arise from the conformational changes in the S_1 excited state.[23] The minor contribution by the conformational change in the S_1 excited states of Z2, Z3, and Z4 becomes manifest upon photoexcitation at 420 nm, exhibiting ~8 ps time constants. The conformational heterogeneity is caused by the dihedral angle distribution between the adjacent porphyrin moieties. The dihedral angle between porphyrin rings in the multiporphyrin arrays investigated in this work is most likely to reside at 90° to maintain orthogonal conformation due to a large steric hindrance imposed by the direct linkage between bulky porphyrin rings. For these multiporphyrin arrays, rotation about the meso-meso C−C bond is expected to be substantially hindered, and as a consequence the coplanarity of the porphyrin rings cannot be achieved. In order to gain further insight into the dihedral angle distribution in this series of porphyrin arrays at ambient temperature, we carried out semiempirical calculation with AM1 Hamiltonian. First, we performed geometry optimization for the monomer (Z1), which was used subsequently to construct the Z2 dimer with meso-meso C−C bond length set equal to 1.54 Å and various dihedral angles. Then we calculated the total energy of the Z2 dimer as a function of dihedral angle. The calculation data can be used to infer some of the conformational properties of the arrays. As seen in Figure 4, the initial conclusions are that the dihedral angle distribution is about 90° ± 20° at ambient temperature because kT value at room temperature is approximately 25 meV. As expected, the dihedral angle distribution is somewhat narrow, but not so rigid probably because of the lack of peripheral substituents at β positions of porphyrin rings. The pliability toward rotation about the meso-meso C−C bond suggests that the heterogeneity in the ground state conformers in these arrays is possible, although its contribution seems to be not so large as revealed in our calculation. Indeed, the contribution by the heterogeneity of this series of samples to the subsequent ~8 ps decay components

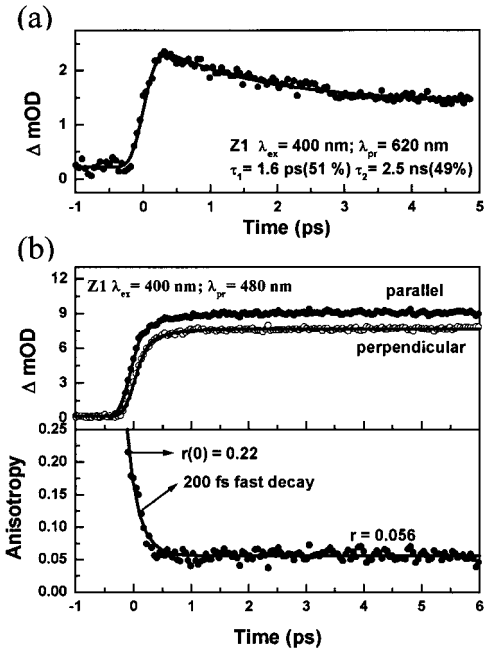

Figure 5. (a) Magic angle transient absorption profile for Z1, probed at 620 nm after the photoexcitation at 400 nm; decay time constants and normalized amplitude (in parentheses) are as follows: $\tau_1 = 1.6$ ps (51%), $\tau_2 = 2.5$ ns (49%). (b) Comparison of transient absorption signals of Z1 for parallel and perpendicular orientation of pump and probe polarization at 480 nm probe wavelength following 400 nm excitation and the time dependence of anisotropy ($r_0 = 0.22$, $\tau = 200$ fs, $r_\infty = 0.056$).

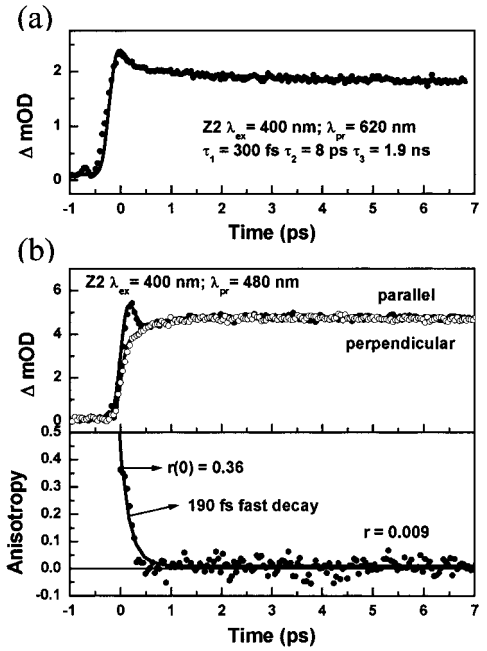

Figure 6. (a) Magic angle transient absorption profile for Z2, probed at 620 nm after the photoexcitation at 400 nm; $\tau_1 = 300$ fs, $\tau_2 = 8$ ps, $\tau_3 = 1.9$ ns. (b) Comparison of transient absorption signals of Z2 for parallel and perpendicular orientation of pump and probe polarization at 480 nm probe wavelength following 400 nm excitation and the time dependence of the anisotropy ($r_0 = 0.36$, $\tau = 200$ fs, $r_\infty = 0.009$).

after the initial rise in the overall fluorescence temporal profile is not so significant as indicated by the relatively small amplitudes of these fast decaying components in Z2, Z3, and Z4.

Ultrafast Transient Anisotropy Decay Dynamics. The magic angle transient absorption dynamics of Z1 was obtained using 400 nm excitation (Figure 5a). As expected, the transient absorption difference signal at 620 nm is dominated by transient absorption with an instantaneous rise. The temporal profile at this wavelength exhibits a short initial decay ($\tau = 1.6$ ps) and a subsequent long decay ($\tau = 2.5$ ns). The time constants obtained from transient absorption profile are consistent with those derived from fluorescence decay measurements, indicating that these two time constants are respectively responsible for S_2-S_1 internal conversion and S_1 state decay processes. Photoexcitation at 400 nm initially populates the S_2 excited state, which decays to the lowest energy excited emitting S_1 state. Thus, the observed 1.6 ps internal conversion time determined from magic angle detection for Z1 reflects the sum of the rates of all relaxation pathways between components of the S_2 and S_1 levels. But it does not provide information regarding the rate constants of the individual processes such as intramolecular vibrational redistribution, vibrational cooling and so on.[38,39]

The anisotropic transient dynamics for monomeric Z1 at 480 nm after photoexcitation at 400 nm are also shown in Figure 5b. In the present case, the experimental anisotropy does not contain any indication of $x-y$ coherence (i.e., values of $r_0 > 0.4$ or < -0.2);[40,41] we therefore conclude that dephasing is complete on a time scale faster than the temporal resolution of our measurements. A single-exponential (~200 fs) depolarization of the transient absorption signal is observed from the initial value $r_0 = 0.22$ to a final value r_∞ of 0.056. A similar behavior was observed for Zn(II)TPP ($t = 400$ fs, $r_0 = 0.28$, $r_\infty = 0.08$).[23] Thus, this time constant is in a good accordance with equilibration of an incoherent S_2 state having a nonstatistical mixture of near-degenerate B_x and B_y components, which leads to a final anisotropy value of ~0.1 as the initial population becomes randomized between the orthogonal states. The initial anisotropy is lower than the expected value of 0.4 for monomeric porphyrin complexes, possibly as a consequence of accessing transitions with the probe pulse with different anisotropies.[41]

Figure 6a displays the transient absorption decay dynamics of Z2 detected at magic angle, illustrating the initial fast decay (~300 fs) component followed by a relatively short-lived one (~8 ps) on the plateau of the long-lived component (1.9 ns). The time constant of the initial fast decay is in good accordance with the value obtained as the rise component in the fluorescence up-conversion experiment of Z2, indicative of the fast $S_2 \rightarrow S_1$ internal conversion processes. The ~8 ps decay component is the same as the initial fast decay in the fluorescence up-conversion signal of Z2. Thus, it seems to reflect the conformational change in the excited S_1 state.

The transient anisotropy decay of Z2 was measured at 480 nm after photoexcitation at 400 nm, which reveals a decay of the transient absorption anisotropy to a final value of almost zero on a time scale of 200 fs (Figure 6b). This anisotropy decay process is believed to arise from two processes: the equilibration between the degenerate B_x and B_y components of the S_2 state of a single porphyrin moiety within the dimer and the incoherent energy hopping[42] between the porphyrin constituents in the dimer. The contribution by the latter process seems to be more significant, because the initial anisotropy value (r_0) of 0.36 in Z2 at 480 nm is larger than that of Z1 ($r_0 = 0.22$), indicating the relative orientation of porphyrin constituents in Z2 arrays remains orthogonal to each other. The final anisotropy value close to zero is in a good agreement with equilibration among states with noncoplanar transition moments, as expected for an orthogonal orientation of the porphyrin rings for Z2 dimer.

Figure 7a shows the transient absorption decay profiles of Z3 at 490 nm with magic angle detection. The initial fast decay

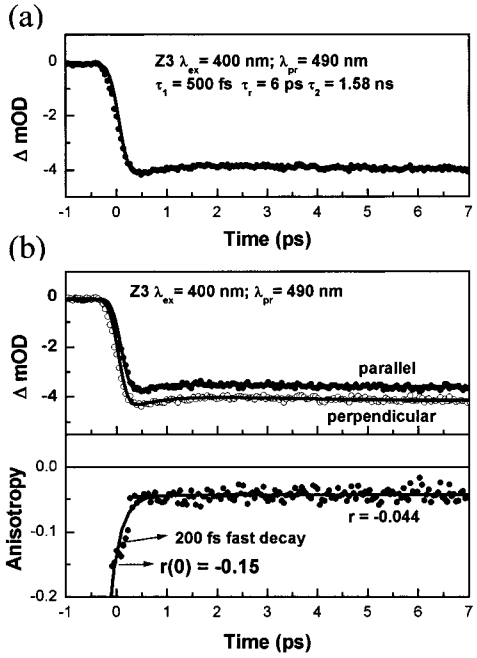

Figure 7. (a) Magic angle transient absorption profile for Z3, probed at 490 nm after the photoexcitation at 400 nm; $\tau_1 = 500$ fs, $\tau_2 = 6$ ps, $\tau_3 = 1.58$ ns. (b) Comparison of transient absorption signals of Z3 for parallel and perpendicular orientation of pump and probe polarization at 490 nm probe wavelength following 400 nm excitation and the time dependence of the anisotropy ($r_0 = -0.15$, $\tau = 200$ fs, $r_\infty = -0.044$).

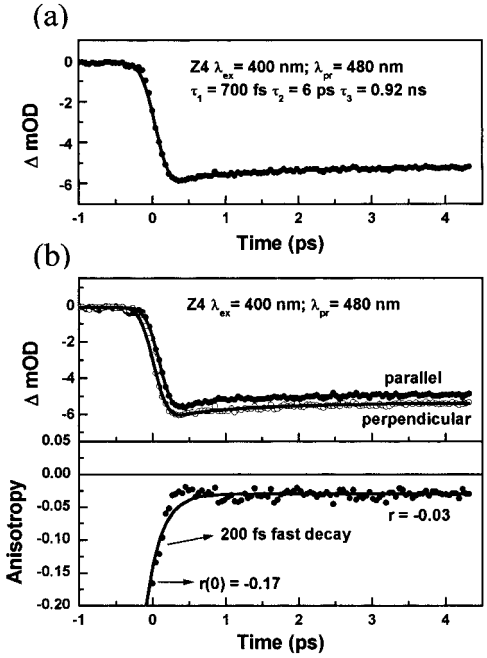

Figure 8. (a) Magic angle transient absorption profile for Z4, probed at 480 nm after the photoexcitation at 400 nm; $\tau_1 = 700$ fs, $\tau_2 = 6$ ps, $\tau_3 = 0.92$ ns. (b) Comparison of transient absorption signals of Z4 for parallel and perpendicular orientation of pump and probe polarization at 480 nm probe wavelength following 400 nm excitation and the time dependence of the anisotropy ($r_0 = -0.17$, $\tau = 200$ fs, $r_\infty = -0.03$).

process (500 fs) seems to represent the fast $S_2 \rightarrow S_1$ internal conversion process followed by a relatively short-lived decay (~6 ps). The ~6 ps decay time constant may be suggested to be a conformational change in the S_1 state, as revealed to have ~6 ps lifetime in the fluorescence up-conversion measurement. The anisotropic decay profile having the initial fast decay (~200 fs) is shown in Figure 7b. The initial anisotropy value r_0 is about −0.15, meaning that the dipole transition angle between 490 nm probe and 400 nm photoexcitation is nearly orthogonal each other.

In the transient absorption temporal profile at 480 nm with magic angle detection of Z4 (Figure 8a), the initial fast decay component (~700 fs), which is observed as the rise in fluorescence up-conversion, can be suggested to be the $S_2 \rightarrow S_1$ internal conversion. The subsequent relatively short rise with approximately 6 ps time constant seems to appear in the temporal profile, but the relative contribution of this process is not so significant. This component is also believed to arise from the conformational change in the excited S_1 state as seen in the fluorescence up-conversion measurement. The fast anisotropic decay of Z4 is very similar to that of Z3 (Figure 8b), indicative of the facilitated incoherent energy hopping processes between porphyrin ring units. In the case of Z2, Z3, and Z4, the increased number of porphyrin ring moieties could make the transition dipole along the long axis more enhanced while the transition dipole lies on the molecular plane in monomeric porphyrin, Z1.

IV. Discussion

Steady-State Fluorescence Anisotropy. Different values of the fluorescence excitation anisotropy result from different relative orientations of the absorption and emission transitions within the chromophore. According to Kasha's rule,[43] the lowest singlet excited state is responsible for the fluorescence irrespective of initially populated state in the aromatic compounds. Thus, we can expect only slight, if any, change in the emission dipole irrespective of excitation wavelength. Therefore, most of excitation wavelength dependence of anisotropy value, which is influenced by both absorption and emission transition dipoles, is thought to result from the change in absorption dipole. The relative absorption transition dipole angle at high-energy exciton B band (S_2) is different from that at low-energy exciton split B band (S_2') in Z2, Z3 and Z4 as seen in the difference in the fluorescence excitation anisotropy values between these two bands (Figure 2 and Table 1).

Photoexcitation of the conjugated porphyrin arrays features a meso-to-meso linkage topology at around 400 nm, and thus accesses a state which is polarized orthogonal to the $S_0 \rightarrow S_1$ transition. This indicates that energy transfer between each constituent in these arrays will randomize the excitation between two porphyrin rings oriented in almost 90°. The absorption spectra of porphyrin array complexes are consistent with the presence of several overlapping transitions in the Soret region, thus serving as the possible cause of this deviation from the expected fluorescence anisotropy value for a perpendicular transition moment (−0.2). On the other hand, the Q-band excitation of these porphyrin arrays always exhibits positive anisotropy values, indicating that the orientation angle difference between absorption and emission transition dipoles is small (Table 1). Thus, the positive anisotropy value for the low-energy exciton split Soret band indicates that the relative orientation of the transition dipole for this transition is similar to that for the Q-band transition, whereas the high-energy Soret transition is close to the localized electronic one. In other words, the high-energy Soret band does not arise from the exciton splitting but from the residual monomeric Soret band transition. The high-energy exciton split Soret band, which is expected to occur at higher energy than that of monomer Soret band, seems to be dipole forbidden transition (very low oscillator strength (dark state)) due to the orthogonal orientation between adjacent porphyrin units. In order to confirm this feature, the directly linked porphyrin dimer is bridged by substituting additional

linkers ($-O-(CH_2)_n-O-$, $n = 1, 2, 3, 4, 6, 8, 10$) on meso phenyl group of each monomeric porphyrin unit. This series of dimers gives rise to a gradual change in the dihedral angle between the adjacent porphyrin units with a variation in the length of linker ($n = 1, 2, 3, 4, 6, 8, 10$). For instance, when $n = 10$, this bridge becomes flexible with almost no restriction on the diheral angle to maintain orthogonal configuration between the neighboring porphyrins. On the other hand, when $n = 1$, there is a significant restriction on the diheral angle to result in a perturbation in the orthogonal configuration between the adjacent porphyrin units. In this case, the high-energy exciton split Soret band is clearly seen to the blue side of the monomeric unshifted Soret band in addition to the low-energy exciton split Soret band to the red side of the monomeric Soret band. In this case, the monomeric Soret band is still observed with almost the same intensity as the exciton split Soret band. This indicates that the unshifted Soret bands around at 415 nm in the series of directly linked porphyrin arrays originated from the residual monomer Soret transitions. Thus, the negative anisotropy value for this band can be explained in terms of the localized monomeric electronic character in contrast with the delocalized electronic nature of the low-energy exciton split Soret band.

The larger positive values of anisotropy on the order of Z2, Z3, and Z4 suggest that the transition dipoles are expected to be oriented along the long axis of the linear porphyrin arrays as the molecular size becomes larger. As a consequence, the angle difference between absorption and emission dipoles becomes smaller to result in a large positive anisotropy value.

Fluorescence Anisotropy Decay. When a molecular system is irradiated with a polarized light, only molecules whose transition dipole moments lie parallel to the direction of the light polarization are excited and the subsequent fluorescence yields the same polarization as the initial excitation light. However, if the excited molecules undergo reorientational motions before they fluoresce or the excitation energy is transferred to nearby molecules with different orientations, the degree of polarization decreases. Any processes which disturb initial orientations of the excited molecules will result in the fluorescence depolarization (FD). The FD study provides information on molecular motions and intermolecular interactions. Time-resolved FD has been measured to study the rotational motion and electronic dynamics such as excitation energy transfer in various ordered and disordered systems. The fluorescence anisotropy decay, $r(t)$, offers detailed information on the diffusive motions of the fluorophore.[44] In general, $r(t)$ exhibits multiexponential decay rates due to anisotropic rotations with respect to its three molecular axes. If we approximate the molecular shape as a sphere, the decay of fluorescence anisotropy becomes a single-exponential decay with its decay rate proportional to the rotational diffusion rate. Therefore, slower fluorescence anisotropy decay is expected for larger molecules because of the solute−solvent friction and the molecular shape. As seen in Figure 2, the fluorescence anisotropy decay rate is found to decrease with an increase in the number of porphyrin rings.

More specifically, porphyrin monomer is a disklike molecule and one may expect the in-plane rotations to be more rapid than the out-of-plane rotations. The out-of-plane motion must displace the plane of the molecule, which requires the displacement of solvent molecules. The in-plane rotations probably require less displacement of solvent and thus they are expected to be more rapid. Such a molecule is referred to as being nonsymmetrical and its rotations are said to be anisotropic. Thus, upon increasing the number of porphyrin molecules, these oligomers become nonsymmetric, so one does not expect equal rotational rates in all directions. As the overall molecular shape is elongated on the order of Z2, Z3, and Z4, the molecular rotation perpendicular to the long axis experiences more restriction from the surrounding solvent molecules to exhibit the slower rotational diffusion rate. In addition, the in-plane rotational contributions to the overall rotational diffusion motion are less significant upon increasing the number of porphyrin units, and consequently the overall anisotropic decay rates become slower as shown in Figure 2. The decay of the fluorescence anisotropy appeared to be slightly dependent on the excitation wavelength. This result can be explained in terms of the local heating of the solvent by excess vibrational energy upon higher energy excitation.[45]

Ultrafast Fluorescence Decay of Z1, Z2, Z3, and Z4. There is a relatively large energy separation in metalloporphyrins between the S_2 and S_1 excited states, which appears as Q and B bands in UV−visible region. In addition, these two states are considered as a 50−50 admixture of two common excited electronic configurations $^1(a_{1u},e_g)$ and $^1(a_{2u},e_g)$ in accidental degeneracy, and the energy surfaces of the S_1 and S_2 excited states are almost parallel. This definitely retards the $S_2 \rightarrow S_1$ intramolecular electronic internal conversion processes.[34] The emitting state of the monomeric porphyrin Z1 is formed with a 1.6 ps time constant following Soret band excitation and decays on a slow time scale of 2.5 ns. The vibrational cooling process that is the dissipation of excess vibrational energy through solute−solvent bath interaction in similar closed-shell metalloporphyrin monomers has been observed to lead to a spectral evolution on a 10−20 ps time scale.[36] Thus, the contribution of this relatively slow process to the initial decay of the transient fluorescence temporal profiles in our time window is negligible.

The transient dynamics observed for the porphyrin oligomers is in contrast with that observed for Z1. Formation of the emitting state occurs on a faster time scale for Z2, Z3, and Z4 than for Z1; we note that a similar observation was made for a porphyrin μ-oxo dimer,[46] which was ascribed to an energy transfer process that occurred between the B- and Q-states of adjacent chromophores. The large splitting observed in the B-band region of these oligomers indicates a significant perturbation of the B-state electronic wave functions, while the absence of any perceptible splitting in the Q-band region suggests that the Q-states of the dimer are only weakly perturbed relative to the monomer.[47] These observations suggest that the Franck−Condon factors for $B \rightarrow Q$ internal conversion in the oligomers are substantially different from those for the monomer, and hence possibly more favorable for nonradiative $S_2 \rightarrow S_1$ decay. Additionally, the splitting of the component levels of the S2 manifold establishes a band of intermediate levels between the state accessed by 400 nm excitation and the emitting state. This provides a "ladder" for sequential relaxations between successive pairs of levels that are separated by energies much smaller than the S_2-S_1 gap of conventional porphyrin monomers and less strongly coupled porphyrin arrays (typically 7000−10 000 cm^{-1}). The $S_2 \rightarrow S_1$ internal conversion processes for compounds Z2, Z3, and Z4 are facilitated by improved Franck−Condon factors with respect to the monomeric building blocks, because the highly split S2 levels for Z2, Z3, and Z4 provide a large number of closely spaced intermediate states that enhance these processes.

The increased rise times in Z2, Z3, and Z4 fluorescence compared with the Z1 fluorescence indicate that the internal conversion and the vibrational energy relaxation in the S_1 states manifolds are believed to become faster due to the existence of ladder-type deactivation channel. According to the energy gap

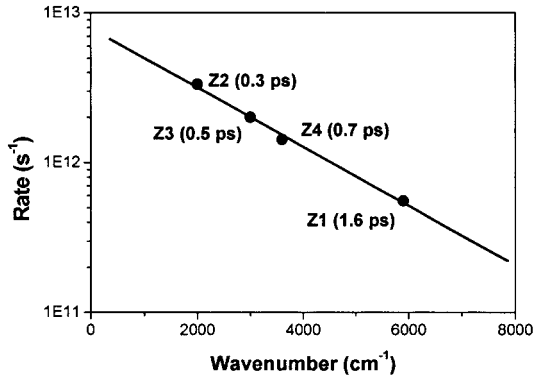

Figure 9. Plot of Log (internal conversion rate) vs the energy gap between the high-energy Soret band and the low-energy exciton split Soret band ($S_2 - S_2'$) for Z2, Z3, and Z4. As for monomer Z1, the energy gap between the Soret and Q-bands ($S_2 - S_1$) was used.

law, the internal conversion rate can be given as $k_{IC} \sim 10^{13} \exp^{-\alpha\Delta E}$ with α and ΔE being the proportionality constant and the energy gap between the two electronic states, respectively. We plot the log value of internal conversion rate vs the energy gap between the high-energy monomeric Soret band (S_2) and the low-energy exciton split Soret band (S_2'), because the $S_2' \rightarrow S_1$ internal conversion is believed to be much faster than the $S_2 \rightarrow S_2'$ process. We can find the linear relationship with the proportionality constant α as 2.0×10^{-4} (Figure 9). The rate-determining step in the overall internal conversion processes upon photoexcitation to the S_2 states in porphyrin arrays is likely to be the $S_2 \rightarrow S_2'$ internal conversion process, because the S_2' state is the delocalized excitonic state being similar to the S_1 state in delocalization feature in contrast with the monomeric localized electronic feature of the S_2 state. Hence the electronic coupling between S_2' and S_1 states is suggested to be much stronger as compared with that between S_2 and S_2' states. On the other hand, the solvation dynamics in these types of porphyrin oligomers, if any, is likely to be represented by the fast dynamic red shift of the emission exhibiting biexponential kinetics with few hundred femtoseconds and few picosecond time scales representing solvent reorganization along respective inertial and diffusive solvent coordinates.[48] But the relatively nonpolar porphyrin moieties and nonpolar toluene solvent employed in the present work do not seem to induce a large polarizability change in the S_1 excited states of Z2, Z3, and Z4.[49,50] To give a clear picture of the ultrafast photoexcitation dynamics in porphyrin arrays, the schematic potential energy diagram with corresponding dynamics is presented in Figure 10.

No significant perturbation in the steady-state Q-band spectral absorption, in contrast with a large split in the Soret band region, indicates a weak electronic communication among the constituent porphyrin pigments in the ground state mainly due to the orthogonal arrangement of the porphyrin rings in these arrays. No evidence is seen in the steady-state Q-band absorption region to suggest conformational heterogeneity. Thus, if significantly different ground-state conformers existed, they would be spectrally indistinguishable, which is highly unlikely. But the existence of the nonorthogonal conformers in solution is believed to result in a slight reduction in the dihedral angle from the perpendicular arrangement of the porphyrin constituents. This conformational change is likely to induce a slight increase in electronic π-conjugation over the entire porphyrin arrays. The contribution to the overall dynamics by the conformational heterogeneity in Z2, Z3, and Z4 is not so significant as indicated by the relatively small amplitudes of ~8 ps decay components

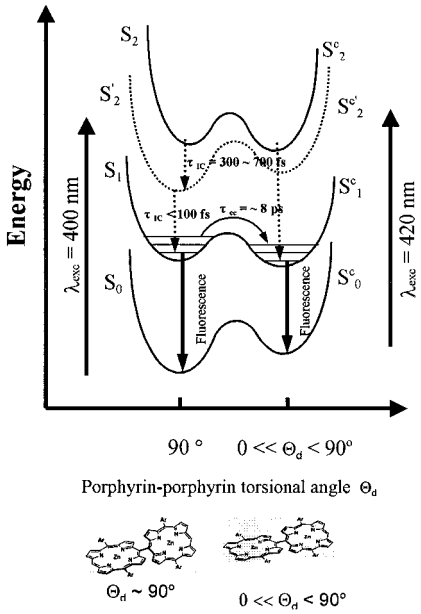

Figure 10. Schematic potential energy diagram for porphyrin arrays investigated in this work to illustrate the energy relaxation dynamics. S_0, S_1, S_2', and S_2 represent the ground state, the lowest emitting Q state, the low-energy exciton split B state, and the high-energy exciton B state, respectively. τ_{IC} and τ_{cc} represent the internal conversion and the conformational change in the S_1 state, respectively. The superscript "c" on the state representation denotes the conformer.

in the transient fluorescence signals. This fact also suggests that a strong steric hindrance imposed by the directly linked porphyrin rings result in the orthogonal orientation of the adjacent porphyrin rings to reduce significantly the possibility of the existence of conformers. Although the time scale for this process is similar to that for the vibrational cooling, the photoexcitation wavelength dependence on the amplitude of ~8 ps decay or rise component in the fluorescence up-conversion signal is likely to support the conformational change in the S_1 states of Z2, Z3, and Z4. The steady-state fluorescence spectra exhibit a slight difference in the spectral features with a change in photoexcitation wavelengths possibly due to the existence of the heterogeneous conformers expected to have slightly different absorption transition energies (not shown). The time constants we observed in Z2, Z3, and Z4 for the conformational change in the S_1 state manifolds are consistent with approximately 30 ps time constants for the similar processes found in the highly conjugated ethyne-bridged zinc(II)porphyrin dimer and trimer.

After the formation of the vibrationally ground S_1 state, the relaxation processes decaying to the ground state appear as fluorescence decays with lifetimes of 2.57, 1.93, 1.58, and 0.97 ns in Z1, Z2, Z3, and Z4, respectively, as measured by the TCSPC method. In a large molecule with a higher density of background levels, the fluorescence decays more rapidly since the excitation energy is dissipated into a large number of accessible states.[38] The increase in the degrees of freedom, which leads to the higher density of molecular states, is responsible for the observed shorter fluorescence lifetimes on the order of Z1, Z2, Z3, and Z4. In addition, since there is a higher density of background levels in large molecules, the vibronic emission band becomes less resolved with an increase in the number of porphyrin rings. The overall photoexcitation dynamics occurring in these molecular arrays are summarized in Figure 10.

Ultrafast Transient Anisotropy Decay Dynamics. In the case of a molecule with a 4-fold symmetry axis such as

porphyrin, the $|x\rangle$ state will have a different energy from the $|y\rangle$ state for a given solvent configuration. Fluctuations in the local solvent configuration will give rise to fluctuations in the molecular parameters such as energy and coupling constant between two states. The decay associated with the coupling and energy fluctuations contributes to the overall transient anisotropy decay.[41] The energy fluctuations will give rise to the dephasing of two transitions whereas the coupling fluctuation will give rise to the flow of population between these two states. As the level pair is excited from the ground state by a δ-function optical pulse and probed by another such pulse to either the ground state or another excited state, the resulting anisotropy of the pump−probe signal can then be written in the suggestive form based on the previous work by Wynne et al.[41]

$$r(t) = 0.7e^{-\gamma t} + 0.4(e^{-2\Gamma t} - e^{-\gamma t}) + 0.1(1 - e^{-2\Gamma t})$$

where γ represents the decay caused by the energy fluctuations and Γ is the decay associated with the coupling fluctuations. The first term is the decay of the fully coherent ensemble from the anisotropy of 0.7, the second term is the rise and decay of a partially coherent ensemble with an anisotropy of 0.4, and the last term represents the evolution of the dephased ensemble. In other words, at very short times before dephasing starts to contribute, the anisotropy has a value of 0.7. Then it decays to the value of 0.4 mainly due to the electronic dephasing. After the level pair is completely dephased, the anisotropy attains a value of 0.1.

Wynne et al.[40] reported that the emission of the initially prepared MgTPP electronically coherent excited-state ensemble decayed with three time constants: 210 fs, 1.6 ps, and 100 ps. The fast (210 fs) time constant corresponds to the loss of coherence between the Q_x and Q_y components of the E_u excited state of porphyrin; the second fastest constant (1.6 ps) corresponds to the decay of an incoherent Q_x, Q_y ensemble having a nonstatistical mixture of Q_x and Q_y populations. The slowest decay is simply the reorientation time of the electronically dephased E_u excited state of MgTPP. In the present case, the experimental anisotropy does not contain any indication of $x-y$ coherence (i.e., values of $r_0 > 0.4$ or < -0.2); we therefore conclude that dephasing is complete on a time scale faster than the temporal resolution of our measurements. Therefore, the 200 fs depolarization of anisotropy observed for Z1 is caused by incoherent population transfer between the B_x and B_y components of the E_u excited state, which are coupled by the random electric fields established by the fluctuating solvent environment.

In the transient anisotropy decay of dimer, the additional condition that the x and y polarized transitions have an intensity ratio of $(1 + \cos\theta)/(1 - \cos\theta)$ should be included, where θ is the angle between the transition dipoles in each half. The dimer anisotropy with a certain anlgle θ is given as follows:[51]

$$r_D(t) = \frac{r(t) + \frac{1}{10}[3 + e^{-\gamma t} - 3f(t)]\cos^2\theta}{1 + e^{-\gamma t}\cos^2\theta}$$

where

$$f(t) = \left[\frac{\gamma}{2\Omega}\sin(\Omega t) + \cos(\Omega t)\right]e^{-at}$$

$$\Omega^2 \equiv b^2 - a^2, \quad a \equiv 2\Gamma + \gamma/2, \quad b^2 \equiv 4\beta^2 + 2\Gamma(2\Gamma + \gamma)$$

where β is the static coupling constant.

In our directly linked porphyrin dimer, the anisotropy decay follows roughly the monomer $r(t)$, because the angle θ between transition dipoles residing at each monomeric unit is close to the dihedral angle of almost 90° as determined by the AM1 calculation.

The initial anisotropy value of 0.36 (i.e., values of $-0.2 < r_0 < 0.4$) in Z2 dimer in the transient anisotropy decay suggests that the excitation exchange coupling fluctuations seem to be large in the present case, implying that the contribution of coupling fluctuations to the anisotropy decay is not negligible as compared with the energy fluctuations of the two moieties. This is in contrast with the case of 9,9′-bifluorene,[28b] where the energy fluctuations of the two fluorene units are predicted to dominate the decay resulting from a weak excitonic coupling between two moieties. The exciton coupling energy between neighboring porphyrins is larger than that found for 1,4-phenylene-bridged porphyrin arrays when considering the energy splitting of B band (Figure 1) in Z2−Z4 absorption spectra. The exciton coupling in Q-bands of Z2−Z4 is much smaller than in B band. The observed small electronic interactions in Z2−Z4 are indicative of the fact that these porphyrin units are nearly orthogonal to each other due to a large steric hindrance. In other words, the dihedral angle between porphyrin moieties is estimated to nearly be 90° while the exact structures of Z2−Z4 have not been reported yet.

In monomeric porphyrin Z1, the long time anisotropy in the transient anisotropy decay has the positive value ($r = 0.056$), meaning that the transition dipole direction of B state, which is certainly on the porphyrin plane, does not have a considerable deviation from those of the detected states. On the other hand, in porphyrin arrays the transition dipole direction seems to be enhanced along the long axis of Z2, Z3, and Z4 due to the exciton delocalization induced by the fast energy hopping processes within 200 fs after photoexcitation of the localized B state at 400 nm. This process is considered to induce the exciton delocalization from the initially localized S_2 state accessible by 400 nm excitation to the delocalized S_1 state. This seems to be facilitated as the number of porphyrin rings increases as demonstrated by the higher initial anisotropy values.

V. Summary and Conclusions

The motivation for the molecular design of directly linked porphyrin arrays to mimic the light-harvesting arrays is toward that the porphyrins must be brought closer to permit rapid energy transfer. To gain further insight into the energy flow mechanism and its relationship with molecular geometry and the number of pigments in the directly linked porphyrin, arrays up to four porphyrin units were investigated by employing various transient spectroscopic methods.

The steady-state excitation anisotropy spectra of Z2, Z3, and Z4 porphyrin arrays show that the photoexcitation of the high-energy Soret band induces a large angle change between absorption and emission dipoles in contrast with the photoexcitation of the low-energy exciton split Soret and Q-bands. This result indicates that the high-energy exciton Soret band exhibits the localized monomeric character with its dipole moment deviated from the array chain direction, while the low-energy exciton split Soret band is delocalized through the array chain. As the number of porphyrin rings increases, the fluorescence lifetimes decrease since the energy relaxation process is facilitated by energy dissipation into a large number of accessible states. The fluorescence anisotropy decay measurements reveal that the rotational diffusion rates become slow as the number of porphyrin rings increases. As the overall molecular shape is elongated along the direction of the addition of porphyrin units, the out-of-plane rotation experiences a large

displacement of solvent molecules to result in a slow rotational diffusion motion.

Ultrafast fluorescence up-conversion measurements illustrate that the internal conversion from the highly excited electronic states to the lowest excited emitting state is facilitated in Z2, Z3, and Z4 through the ladder-type deactivation channel as compared to the relatively slow internal conversion of 1.6 ps in monomeric porphyrin. The internal conversion rate dependence on Z1, Z2, Z3, and Z4 can be well explained by the energy gap law. Femtosecond transient absorption experiments with magic angle and different polarization in probe beam were also carried out in order to observe the energy relaxation and anisotropy dynamics at the initial stage of exciton migration process upon photoexcitation. The internal conversion process is accompanied by the incoherent energy hopping processes as evidenced by a large change in the anisotropy value at the initial stage of the transient absorption temporal profile after photoexcitation. In addition, the decay or rise components with approximately 8 ps time constant were observed in both fluorescence up-conversion and femtosecond transient absorption decays, although the contribution of these components to the overall temporal profiles is not so significant. These components are believed to arise from the conformational change in the excited states, because the dihedral angle distribution in these arrays was estimated to be 90° ± 20° at ambient temperature based on the AM1 calculation.

Collectively, our data from various steady-state and transient spectroscopic measurements should provide a complete picture of the energy migration processes in the arrays. Ultimately, our studies will be extended to the controlled dihedral angle molecular systems by substituting different size of linkers groups on the constituent monomer units. These investigations are currently underway.

Acknowledgment. This work has been financially supported by the National Creative Research Initiatives of the Ministry of Science & Technology of Korea (D.K.). S.K.K. acknowledges the support of this work by the Basic Science Research Institute Program (BSRI-98-3413). The work at Kyoto was supported by Grant-in-Aids for Scientific Research from the Ministry of Education, Science, Sports and Culture of Japan and by CREST (Core Research for Evolutional Science and Technology) of Japan Science and Technology Corp. (JST).

Supporting Information Available: Molecular structure, fluorescence decay profiles, and fluorescence spectra of Z1, Z2, Z3, and Z4. This material is available free of charge via the Internet at http://pubs.acs.org.

References and Notes

(1) (a) *Photosynthetic Light-Harvesting Systems*; Scheer, H., Schneider, S., Eds.; de Gruyter: Berlin, 1988. (b) Pearlstein, R. M. In *Chlorophylls*; Scheer, H., Ed.; CRC Press: Boca Raton, FL, 1991; p 1047. (c) Sundström, V.; van Grondell, R. In *Chlorophylls*; Scheer, H., Ed.; CRC Press: Boca Raton, FL, 1991; p 1097. (d) van Grondell, R.; Dekker, J. P.; Gillbro, T.; Sundström, V. *Biochim. Biophys. Acta* **1994**, *1187*, 1. (e) Sundström, V.; Pullerits, T.; van Grondelle, R. *J. Phys. Chem. B* **1999**, *103*, 2327.

(2) (a) Deisenhofer, J.; Epp, O.; Miki, K.; Huber, R.; Michel, H. *J. Mol. Biol.* **1984**, *180*, 385; *Nature (London)* **1985**, *318*, 618. (b) Chang, C.-H.; Tiede, D.; Tang, J.; Smith, U.; Norris, J.; Shiffer, M. *FEBS Lett.* **1986**, *205*, 82. (c) Scherer, P. O. J.; Fischer, S. F. In *Chlorophylls*; Scheer, H., Ed.; CRC Press: Boca Raton, FL, 1991; p 1079. (d) Parson, W. W. In *Chlorophylls*; Scheer, H., Ed.; CRC Press: Boca Raton, FL, 1991; p 1153. (e) Warshel, A.; Parson, W. W. *J. Am. Chem. Soc.* **1987**, *109*, 6143. (f) Knapp, E. W.; Fischer, S. F.; Zinth, W.; Sander, M.; Kaiser, W.; Deisenhofer, J.; Michel, H. *Proc. Natl. Acad. Sci. U.S.A.* **1985**, *82*, 8463

(3) (a) Andre, J. J.; Holczer, K.; Petit, P.; Riou, M.-T.; Clarisse, C.; Even, R.; Fourmigue, M.; Simon, J. *Chem. Phys. Lett.* **1985**, *115*, 463. (b) Maitrot, M.; Guillaud, G.; Boudjema, B.; Andre, J. J.; Strzelecka, H.; Simon, J.; Even, R. *Chem. Phys. Lett.* **1987**, *133*, 59. (c) Turek, P.; Petit, P.; Andre, J.-J.; Simon, J.; Even, R.; Boudjema, B.; Guillaud, G.; Maitrot, M. *J. Am. Chem. Soc.* **1987**, *109*, 5119.

(4) Hoffman, B. M.; Ibers, J. A. *Acc. Chem. Res.* **1983**, *16*, 15.

(5) (a) Collman, J. P.; Anson, F. C.; Barnes, C. E.; Bencosme, C. S.; Geiger, T.; Evitt, E. R.; Kreh, R. P.; Meier, K.; Pettman, R. B. *J. Am. Chem. Soc.* **1983**, *105*, 2694. (b) Collman, J. P.; Bencosme, C. S.; Barnes, C. E.; Miller, B. D. *J. Am. Chem. Soc.* **1983**, *105*, 2704. (c) Ni, C. L.; Abdalmuhdi, I.; Chang, C. K.; Auston, F. C. *J. Phys. Chem.* **1987**, *91*, 1158.

(6) (a) Gregg, B. A.; Fox, M. A.; Bard, A. J. *J. Phys. Chem.* **1990**, *94*, 1586. (b) Liu, C.-Y.; Pan, H.-L.; Fox, M. A.; Bard, A. J. *Science* **1993**, *261*, 897.

(7) (a) Anderson, H. L.; Martin, S. J.; Bradley, D. D. C. *Angew. Chem., Int. Ed. Engl.* **1994**, *33*, 655. (b) Anderson, H. L. *Inorg. Chem.* **1994**, *33*, 972.

(8) (a) Pellin, M. J.; Wasielewski, M. R.; Kaufmann, K. J. *J. Am. Chem. Soc.* **1980**, *102*, 1868. (b) Bucks, R. R.; Boxer, S. G. *J. Am. Chem. Soc.* **1982**, *104*, 340. (c) Wasielewski, M. R. In *Chlorophylls*; Scheer, H., Ed.; CRC Press: Boca Raton, FL, 1991; p 269. (d) Johnson, D. G.; Svec, W. A.; Wasielewski, M. R. *Isr. J. Chem.* **1988**, *28*, p 193. (e) Johnson, S. G.; Small, G. J.; Johnson, D. G.; Svec, W. A.; Wasielewski, M. R. *J. Phys. Chem.* **1989**, *93*, 5437. (f) Petke, J. D.; Maggiora, G. M. *J. Chem. Phys.* **1986**, *84*, 1640. (g) LaLonde, D. E.; Petke, J. D.; Maggiora G. M. *J. Phys. Chem.* **1988**, *92*, 4746. (h) Thompson, M. A.; Zerner, M. C.; Fajer, J. *J. Phys. Chem.* **1990**, *94*, 3820.

(9) (a) Gouterman, M.; Holten, D.; Lieberman, S. *Chem. Phys.* **1977**, *25*, 139. (b) Chang, C. K. *J. Heterocycl Chem.* **1977**, *14*, 1285. (c) Ichimura, K. *Chem. Lett.* **1977**, 641. (d) Kagan, N. E.; Mauzerall, D.; Merrifield, R. B. *J. Am. Chem. Soc.* **1977**, *99*, 5484. (e) Paine, J. B., III; Dolphin, D.; Gouterman, M. *Can. J. Chem.* **1978**, *56*, 1712. (f) Collman, J. P.; Chong, A. O.; Jameson, G. B.; Oakley, R. T.; Rose, E.; Schmittou, E. R.; Ibers, J. A. *J. Am. Chem. Soc.* **1981**, *103*, 516. (g) Konishin, S.; Hoshino, M.; Imamura, M. *J. Phys. Chem.* **1982**, *86*, 4888. (h) Brookfield, R. L.; Ellul, H.; Harriman, A. *J. Chem. Soc., Faraday Trans. 2* **1985**, *81*, 1837. (I) Kaizu, Y.; Misu, N.; Tsuji, K.; Kaneko, Y.; Kobayashi, H. *Bull. Chem. Soc. Jpn.* **1985**, *58*, 103. (j) Kaizu, Y.; Maekawa, H.; Kobayashi, H. *J. Phys. Chem.* **1986**, *90*, 4234. (k) Osuka, A.; Maruyama, K. *J. Am. Chem. Soc.* **1988**, *110*, 4454. (l) Gurinovich, G. P.; Zenkevich, E. I.; Shulga, A. M.; Sagun, E. I.; Suisalu, A. *Zh. Prikl. Spektrosk.* **1984**, *41*, 446 (in Russian). (m) Zenkevich, E. I.; Shulga, A. M.; Chernook, A. V.; Filatov, I. V.; Gurinovich, G. P. *Teor. Eksp. Khim.* **1989**, p 295. (n) Eriksson, S.; Källebring, B.; Larsson, S.; Mårtensson, J.; Wennerström, O. *Chem. Phys.* **1990**, *146*, 165. (o) Kobayashi, N.; Numao, M.; Kondo, R.; Nakajima, S.; Osa, T. *Inorg. Chem.* **1991**, *30*, 2241. (p) Buchler, J. W.; Knoff, M. In *Optical Properties and Strucure of Tetrapyrroles*; Blauer, G., Sund, H., Eds.; de Gruyter: Berlin, 1985; p 91. (q) Buchler, J. W.; De Cian, A.; Fischer, J.; Kihn-Botulinski, M.; Weiss, R. *Inorg. Chem.* **1988**, *27*, 339. (r) Martin, P. C.; Arnold, J.; Bocian, D. F. *J. Phys. Chem.* **1993**, *97*, 1332. (s) Bilsel, O.; Milam, S. N.; Girolami, G. S.; Suskick, K. S.; Holten, D. *J. Phys. Chem.* **1993**, *97*, 7216. (*t*) Kadish, K. M.; Moninot, G.; Hu, Y.; Dubois, D.; Ibnlfassi, A.; Barbe, J.-M.; Guilard, R. *J. Am. Chem. Soc.* **1993**, *115*, 8153. (u) Collman, J. P.; Prodolliet, J. W.; Leidner, C. R. *J. Am. Chem. Soc.* **1986**, *108*, 2916.

(10) (a) Gasyna, Z.; Kobayashi, N.; Stillman, M. J. *J. Chem. Soc., Dalton Trans.* **1989**, 2397. (b) Dodsworth, E. S.; Lever, A. B. P.; Seymour, P.; Leznoff, C. C. *J. Phys. Chem.* **1985**, *89*, 5698. (c) Ciliberto, E.; Doris, K. A.; Pietro, W. J.; Reisner, G. M.; Ellis, D. E.; Fragala, I.; Herbstein, F. H.; Ratner, M. A.; Marks, T. J. *J. Am. Chem. Soc.* **1984**, *106*, 7748. (d) Yoon, M.; Cheon, Y.; Kim, D. *Photochem. Photobiol.* **1993**, *58*, 31. (e) Markovitsi, D.; Tran-Thi, T.-H.; Even, R.; Simon, J. *Chem. Phys. Lett.* **1987**, *137*, 107. (f) Ohno, O.; Ishikawa, N.; Matsuzawa, H.; Kaizu, Y.; Kobayashi, H. *J. Phys. Chem.* **1989**, *93*, 1713. (g) Kobayashi, N. *J. Chem. Soc., Chem. Commun.* **1991**, 1203. (h) Kobayashi, N.; Lam, H.; Nevin, W. A.; Janda, P.; Leznoff, C. C.; Koyama, T.; Monden, A.; Shirai, H. *J. Am. Chem. Soc.* **1994**, *116*, 879.

(11) (a) Ponomarev, G. V.; Borovkov, V.; Sugiura, K.-I.; Sakata, Y.; Shul'ga, A. *Tetrahedron Lett.* **1993**, *34*, 2153. (b) Senge, M.; Gerzevske, K.; Vicente, M.; Forsyth, T.; Smith, K. *Angew. Chem., Int. Ed. Engl.* **1993**, *32*, 750. (c) Ponomarev, G.; Borovkov, V.; Shul'ga, A.; Sakata, Y. *J. Chem. Soc., Chem. Commun.* **1994**, 1927. (d) Senge, M.; Vicente, M.; Gerzevske, K.; Forsyth, T.; Smith. K. *Inorg. Chem.* **1994**, *33*, 5625. (e) Higuchi, H.; Takeuchi, M.; Ojima, J. *Chem. Lett.* **1996**, 593.

(12) (a) Lin, V. S.-Y.; DiMagno, S. G.; Therien, M. J. *Science* **1994**, *264*, 1105. (b) Lin, V. S.-Y.; Therien, M. J. *Chem.-Eur. J.* **1995**, *1*, 645.

(13) Arnold, D.; Nitschinsk, L. *Tetrahedron* **1992**, *48*, 8781.

(14) Anderson, H. L. *Inorg. Chem.* **1994**, *33*, 972.

(15) Arnold, D.; Nitschinsk, L. *Tetrahedron Lett.* **1993**, *34*, 693.

(16) Vicente, M. G. H.; Smith, K. *J. Org. Chem.* **1991**, *56*, 4407.

(17) Osuka, A.; Liu, B.-L.; Maruyama, K. *Chem. Lett.* **1993**, 949.

(18) Burrell, A.; Officer, D.; Reid, D. *Angew. Chem., Int. Ed. Engl.* **1995**, *34*, 900.

(19) (a) Osuka, A.; Maruyama, K.; Yamazaki, I.; Tamai, N. *Chem. Phys. Lett.* **1990**, *165*, 392. (b) Osuka, A.; Maruyama, K.; Mataga, N.; Asahi, T.; Yamazaki, I.; Tamai, N. *J. Am. Chem. Soc.* **1990**, *112*, 4958.

(20) Yang, S. I.; Lammi, R. K.; Seth, J.; Riggs, J. A.; Arai, T.; D. Kim; Bocian, D. F.; Holten, D.; Lindsey, J. S. *J. Phys. Chem. B* **1998**, *102*, 9426.

(21) Seth, J.; Palaniappan, V.; Johnson, T. E.; Prathapan, S.; Lindsey, J. S.; Bocian, D. F. *J. Am. Chem. Soc.* **1994**, *116*, 10578.

(22) (a) Osuka, A.; Shimidzu, H. *Angew. Chem., Int. Ed. Engl.* **1997**, *36*, 135. (b) Khoury, R. G.; Jaquinod, L.; Smith, K. M. *Chem. Commun.* **1997**, 1057. (c) Ogawa, T.; Nishimoto, Y.; Yoshida, N.; Ono, N.; Osuka, A. *Chem. Commun.* **1998**, 337.

(23) Kumble, R.; Palese, S.; Lin, V. S.-Y.; Therien, M. J.; Hochstrasser, R. M. *J. Am. Chem. Soc.* **1998**, *120*, 11489.

(24) Lee, M.; Kim, D. *J. Opt. Soc. Korea* **1990**, *1*, 52.

(25) Takeuchi, S.; Tahara, T. *J. Phys. Chem. A* **1997**, *101*, 3052.

(26) Jeoung, S. C.; Kim, Y. H.; Kim, D.; Han. J.-Y.; Lee, J.-Y.; Shim, H.-K.; Kim, C. M.; Yoon, C. S. *Appl. Phys. Lett.* **1999**, *74*, 212.

(27) Fleming, G. R. *Chemical Applications of Ultrafast Spectroscopy*; Oxford University Press: Oxford, UK, 1986.

(28) (a) Agranovich, V. M.; Galanin, M. D. *Electronic Excitation Energy Transfer in Condensed Matter*; North-Holland: Amsterdam, 1982. (b) Kim, Y. R.; Share, P.; Pereira, M.; Sarisky, M.; Hochstrasser, R. M. *J. Chem. Phys.* **1989**, *91*, 7557.

(29) Myers, A. B.; Hochstrasser, R. M. *IEEE J. Quantum Electron.* **1986**, *QE−22*, 1482.

(30) Sension, R. J.; Repinec, S. T.; Hochstrasser, R. M. *J. Phys. Chem.* **1991**, *95*, 2946.

(31) Li, M.; Owrutsky, J.; Sarisky, M.; Culver, J. P.; Yodh, A.; Hochstrasser, R. M. *J. Chem. Phys.*, in press.

(32) Hochstrasser, R. M.; Pereira, M. A.; Share, P. E.; Sarisky, M. J.; Kim, Y. R.; Repinec, S. T.; Sension, R. J.; Thorne, J. R. G.; Iannone, M.; Diller, R.; Anfinrud, P. A.; Han, C.; Lian, T.; Locke, B. *Proc. Indian Acad. Sci.* **1991**, *103*, 351.

(33) Cantor, C. R.; Schimmel, P. R. *Biophysical Chemistry Part II Techniques for the Study of Biological Structure and Function;* W. H. Freeman and Co.: San Francisco, 1980.

(34) Kobayashi, H.; Kaizu, Y. In *Porphyrins: Excited States and Dynamics*; Gouterman, M., Rentzepis, P., Straub, K. D., Eds.; ACS Symposium Series 321; American Chemical Society: Washington, DC, 1986; p 105.

(35) (a) Chosrowjan, H.; Tanigichi, S.; Okada, T.; Takagi, S.; Arai, T.; Tokumaru, K. *Chem. Phys. Lett.* **1995**, *242*, 644. (b) Gurzadyan, G. G.; Tran-Thi, T.-H.; Gustavsson, T. *J. Chem. Phys.* **1998**, *108*, 385.

(36) (a) Eom, H. S.; Jeoung, S. C.; Kim, D.; Ha, J.-H.; Kim, Y.-R. *J. Phys. Chem. A* **1997**, *101*, 3601. (b) Rodriguez, J.; Kirmaier, C.; Holten, D. *J. Chem. Phys.* **1991**, *94*, 6020.

(37) (a) Petrich, J. W.; Martin, J. L.; Houde, D.; Poyart, C.; Orszag, A. *Biochemistry* **1987**, *26*, 7914. (b) Petrich, J. W.; Poyart, C.; Martin, J. L. *Biochemistry* **1988**, *27*, 4049. (c) Henry, E. R.; Eaton, W. A.; Hochstrasser, R. M. *Proc. Natl. Acad. Sci. U.S.A.* **1986**, *83*, 8982. (d) Alden, R. G.; Chavez, M. D.; Ondrias, M. R.; Courtney, S. H.; Friedman, J. M. *J. Am. Chem. Soc.* **1990**, *112*, 3241. (e) Alden, R. G.; Ondrias, M. R.; Courtney, S. H.; Findsen, E. W.; Friedman, J. M. *J. Phys. Chem.* **1990**, *94*, 85. (f) Anfinrud, P. A.; Han, C.; Hochstrasser, R. M. *Proc. Natl. Acad. Sci. U.S.A.* **1989**, *86*, 8397. (g) Postlewaite, J. C.; Miers, J. B.; Dlott, D. D. *J. Am. Chem. Soc.* **1989**, *111*, 1248.

(38) (a) Wondrazek, F.; Seilmeier, A.; Kaiser, W. *Chem. Phys. Lett.* **1984**, *104*, 121. (b) Seilmeier, A.; Scherer, P. O. J.; Kaiser, W. *Chem. Phys. Lett.* **1984**, *105*, 140. (C) Gottfried, N. H.; Seilmeier, A.; Kaiser, W. *Chem. Phys. Lett.* **1984**, *111*, 326. (d) Bakker, H. J.; Planken, P. C. M.; Lagendijk, A. *Nature* **1990**, *347*, 745. (e) Green, B. I.; Weisman, R. B.; Hochstrasser, R. M. *Chem. Phys. Lett.* **1979**, *62*, 427. (f) Doany, F. E.; Greene, B. I.; Hochstrasser, R. M. *Chem. Phys. Lett.* **1980**, *75*, 206. (g) Fujimura, Y.; Lin, S. H.; Schröder, H.; Neusser, H. J.; Schlag, E. W. *Chem. Phys. Lett.* **1979**, *43*, 205. (h) Fujimura, Y.; Nakajima, T.; Lin, S. H.; Schlag, E. W. *Chem. Phys. Lett.* **1979**, *67*, 299.

(39) (a) Cho, M.; Fleming, G. R.; Saito, S.; Ohmine, I.; Stratt, R. M. *J. Chem. Phys.* **1994**, *100*, 6672. (b) Moore, P.; Tokmakoff, A.; Keyes, T.; Fayer, M. D. *J. Chem. Phys.* **1995**, *103*, 3325. (c) Fleming, G. R.; Cho, M. *Annu. Rev. Phys. Chem.* **1997**, *47*, 109 and references therein.

(40) (a) Galli, C.; Wynne, K.; Lecours, S. M.; Therier, M. J.; Hochstrasser, R. M. *Chem. Phys. Lett.* **1993**, *206*, 493. (b) Wynne, K.; LeCours, S. M.; Galli, C.; Therien, M. J.; Hochstrasser, R. M. *J. Am. Chem. Soc.* **1995**, *117*, 3749.

(41) Wynne, K.; Hochstrasser, R. M. *J. Raman Spectrosc.* **1996**, *26*, 561.

(42) (a) Sessler, J. L.; Capuano, V. L.; Harriman, A. *J. Am. Chem. Soc.* **1993**, *115*, 4618. (b) Bradforth, S. E.; Jimenez, R.; van Mourik, F.; van Grondelle, R.; Fleming, G. R. *J. Phys. Chem.* **1995**, *99*, 16179. (c) Chachisvilis, M.; Kühn, O.; Pullerits, T.; Sundström, V. *J. Phys. Chem. B* **1997**, *101*, 7275.

(43) Kasha, M. *Discuss. Faraday Soc.* **1950**, *9*, 14.

(44) Lakowicz, J. R. *Principles of Fluorescence Spectroscopy*; Plenum Press; New York, 1983.

(45) *Topics in Fluorescence Spectroscopy*; Lakowicz, J. R., Ed.; Plenum Press: New York, 1991; Vol. I, II.

(46) Ohno, O.; Kaizu, Y.; Kobayashi, H. *J. Chem. Phys.* **1985**, *82*, 1779.

(47) (a) Lin, V. S.-Y.; DiMagno, S. G.; Therien, M. J. *Science* **1994**, *264*, 1105. (b) Lin, V. S.-Y.; Therien, M. J. *Chem. Eur. J.* **1995**, *1*, 645. (c) Angiolillo, P. J.; Lin, V. S.-Y.; Vanderkooi, J. M.; Therien, M. J. *J. Am. Chem. Soc.* **1995**, *117*, 12514.

(48) Horng, M. L.; Gardecki, J. A.; Papazyan, A.; Maroncelli, M. *J. Phys. Chem.* **1995**, *99*, 17311.

(49) Yamazaki, I.; Akimoto, S.; Yamazaki, T.; Shiratori, H.; Osuka, A. *Acta Phys. Polon. A* **1999**, *95*, 105.

(50) (a) Schwarzer, D.; Troe, J.; Votsmeier, M.; Zerezke, M. *J. Chem. Phys.* **1996**, *105*, 3121. (b) Schwarzer, D.; Troe, J.; Zerezke, M. *J. Chem. Phys.* **1997**, *107*, 8380.

(51) (a) Wynne, K.; Hochstrasser, R. M. *Chem. Phys.* **1993**, *171*, 179. (b) Wynne, K.; Gnanakaran, S.; Galli, C.; Zhu, F.; Hochstrasser, R. M. *J. Lumin.* **1994**, *60-61*, 735.